Materials Today: Proceedings xxx (xxxx) xxx

Contents lists available at ScienceDirect

Materials Today: Proceedings

journal homepage: www.elsevier.com/locate/matpr

Deformation behavior of nanostructured aluminum: Experiment and computational study

Surja Deka [a], Farzin Mozafari [b], Ashis Mallick [a,*]

[a] Department of Mechanical Engineering, IIT (ISM) Dhanbad, Jharkhand 826004, India
[b] Department of Mechanical Engineering, Abdullah Gül University, Kayseri, Turkey

ARTICLE INFO

Article history:
Available online xxxx

Keywords:
Ball milling
Nanocrystalline structure
Constitutive model
Finite element

ABSTRACT

Nanocrystalline metals have been processed from powder predecessors in recent times in significant ways, and nowadays, materials are starting to be manufactured which are not only strong but also ductile. Nanocrystalline aluminum (Average grain size 51 nm) was synthesized through high-energy ball milling at the room temperature of microcrystalline powder. The particle size and crystallite sizes were obtained by Williamson Hall and found to be in good correlation with transmission spectroscopy (TEM) data. There was a significant increase in the mechanical properties of nanostructured aluminum in comparison to coarse-grained aluminum. Moreover, a phenomenological model of large-deformation, isotropic, rate-dependent plasticity is developed, which takes into account pressure dependency, plastic dilatation, and non-normal flow. The model has been incorporated into a finite element program. Compression and tension experiments were performed on nanocrystalline aluminum, and the constitutive parameters within the model were estimated from these experiments. The present study shows that the constitutive model successfully simulates the mechanical response of nanocrystalline aluminum with reasonable accuracy using our numerical finite-element capability.

Selection and peer-review under responsibility of the scientific committee of the International Conference on Materials and Manufacturing for Sustainable Developments – 2022.

1. Introduction

Nanocrystalline metals, which have grains < 100 nm, are widely known to have superior properties to their coarse-grained (CG) counterparts and are a primary focus of today's materials research because of their excellent mechanical, electrical, thermal, and chemical properties [1]. When it comes to nanostructured metals, the unique properties of aluminum (Al) make it a vital element due to its lightweight, high strength, and corrosion resistance. Since they possess good corrosion properties, have excellent mechanical properties, can be machined, can be welded, and are relatively inexpensive, they are extensively used in aerospace, automotive, automobile, and construction engineering. There have been many experimental approaches to enhance the strength and ductility of these materials, such as alloying and age hardening. These are two of the most important approaches adopted during the last century [2]. However, an understanding of flow properties and strengthening applied to refinement of grains has recently been found to be a powerful tool for improving their mechanical and functional characteristics. For the past two decades, a variety of methods for processing metals and alloys have emerged, with the primary goal being grain refinement within the submicrometer and nanometer ranges. It is well recognised that grain size is one of the primary instruments for tuning the mechanical characteristics of metallic materials; for instance, the yield strength is correlated with grain size via the well-known Hall-Petch connection [3]. Several recent studies have demonstrated that nanostructuring of aluminum and its alloys can significantly enhance their chemical, mechanical, and thermal properties, making them suitable for functional and structural [4,5].

The literature discusses various methods of producing nanostructured aluminum, including high-pressure torsion, accumulative roll bonding, equal channel angular pressure, high-energy ball milling at cryogenic and room temperatures, and hydrostatic extrusion, chemical vapor synthesis, and electrodeposition [6]. In a recent study by Christudasjustus et al. [7], they synthesized nanocrystalline Al-xV alloys by employing a plasma-assisted high-energy ball milling process. The resulting nc-Al alloy microstructures exhibited grain sizes of less than 50 nm, which

* Corresponding author.
E-mail address: mallick@iitism.ac.in (A. Mallick).

https://doi.org/10.1016/j.matpr.2023.03.577

Selection and peer-review under responsibility of the scientific committee of the International Conference on Materials and Manufacturing for Sustainable Developments – 2022.

invokes the Hall-Petch phenomenon and explains the considerable rise in modulus and microhardness. The nc-Al alloy developed has an elastic modulus of 96.21 GPa and hardness of 5.21 GPa, which is more than several commercially available alloys. Guan et al. [8] examined the effect of milling at the cryogenic temperature on the microstructural evolution and hardness of AZ31 alloy. They noted that after 6 h of milling, the crystallite size was approximately 26 nm. A hardness value of 162 HV was reported, higher than those reported in other AZ31 studies. In Khan's study [9], nc-Al was synthesized by using high-energy ball milling followed by hot consolidation. The results showed that the hardness and strength of nc-Al increased significantly due to the reduction of grain size, i.e., nc-Al possessed a hardness of 230kgf/mm^2 and a high strength of 800 MPa when strained at 2636/s. Nonetheless, the material had a low degree of ductility. As a result, Khan's subsequent research [10] focused on improving the low degree of ductility. He was able to synthesize nc-Al with 50% ductility, but the material strength dramatically decreased to 370 MPa for grains with sizes of 75 nm. Using friction welding, Whalen and his colleagues [11] found that nc-Al had 371 MPa of tensile strength and 16.5% ductility. Therefore, motivated by the above studies, there is a need to synthesize nanocrystalline aluminum, which exhibits a high degree of strength and a reasonable amount of ductility. Therefore, we have proposed to develop a nc-Al with an excellent combination of strength and plasticity under grain refinement by using mechanical milling followed by hot extrusion. Furthermore, a microstructural investigation pertaining to flow stress behavior should be carried out in order to acquire a better understanding of the mechanical behavior of the nc-Al.

Several theoretical frameworks have been proposed for nanostructured metallic materials. Theoretical studies on the mechanical behavior of nanostructured materials can reduce the need for costly experiments and offer a quick way to assess trends that arise with a reduction in grain size. The literature supports investigations on the mechanical behavior of these nanostructured metallic materials using finite element modeling and molecular dynamics simulation. Finite-element modeling of the flow stress behavior of nanocrystalline metals based on the influence of grain size uniformity has been performed by Dobosz and his colleagues [12], and the results show clear evidence of the grain size effect and the reverse Hall-Petch connection. In this regard, another notable contribution was made by Anand [13], wherein he proposed a phenomenological isotropic, large-deformation, rate-dependent elastic–plastic model to predict the mechanical and microindentaion properties of nanocrystalline Mg and Cu. Shimokawa and his colleagues [14] studied intergranular and intragranular deformation's dependence on grain size using molecular-dynamics simulations and found the optimal size of the grain of nc-Al. In another work by Khan et al. [9], he employed the Khan, Huang & Liang model to predict the mechanical response of the nanocrystalline Al by using a bilinear hall patch relation in the viscoplastic constitutive model. Even though there have been studies on the modeling of nc-Al, there have only been a few attempts to predict the flow behavior of these nanostructured materials due to the computational challenges of addressing the boundary and processing conditions. Therefore, the next aim of our study is to provide a reliable modeling framework to model the underlying deformation mechanisms of bulk nc-Al. We have formulated an elastoplasticity constitutive model, which is large-deformation, isotropic, rate-dependent, and where the plastic flow is plastically dilatant, pressure-dependent, and non-normal to model the mechanical responses of nc-Al.

2. Experimental methodology & material characterization

Pure aluminum (Al) powder with a mesh size of 325 and a purity of $\geq$ 99.5% supplied by Sisco Research Laboratories Pvt. Ltd., India. Fig. 1 depicts the FESEM imaging of Al powder particles as received. The ball-to-powder ratio was maintained at 10:1 over the 65-hour mechanical milling process. To prevent aggregation, and cold working of the powders during milling, 1.5 wt% concentration of stearic acid was added as a process control agent (PCA). Then compaction was done on the milled powder at an isostatic pressure of 550 MPa. The compacted billets were then extruded into round bars with a diameter of 8 mm at 450 K.

A high-resolution transmission electron microscope (Talos F200X G2, Thermo Fisher Scientific, United States) and scanning electron microscope (SUPRAM 55 FESEM, Zeiss, Germany) were employed to examine the microstructural evolution of each powder (unmilled and milled powders. The phase components, peaks indexation, and texture evolution of the powders related to milling time were determined by using an X-ray diffractometer (Smartlab, Rigaku, USA). Data were collected with Cu Kα radiation (λ = 0.15 406 nm) and at a step scanning of 4^0/min.

In order to determine crystallite sizes, the peak broadening method was used to measure the Full Width at Half Maximum (FWHM). The Williamson-Hall method, which asserts that the sum of peak broadening (β_T) owing to strain (β_ε) and crystallite size (β_D), was used to measure the crystallite size of the nc-Al. The total broadening is determined by the following equation:

$$\beta_T \cos\theta = \varepsilon(4\sin\theta) + K\lambda/D$$

where, θ is Bragg's angle, K is Scherer's constant, ε is the strain, λ is the wavelength of the incident X-ray, and D is the size of the crystallite.

The tensile experiments of the samples were conducted on a "Hounsfield (50 kN)" instrument. Tensile tests were conducted using a variable crosshead speed of 9.6 mm/min, 0.96 mm/min, and 0.096 mm/min at room temperature. Tensile dog-bone specimens with gauge length and diameter of 16 and 4 mm were prepared.

3. Results and discussion

3.1. Experimental investigation

The nanocrystalline aluminum was synthesized by ball milling the powder for 65 h followed by in situ hot extrusion. A broadening

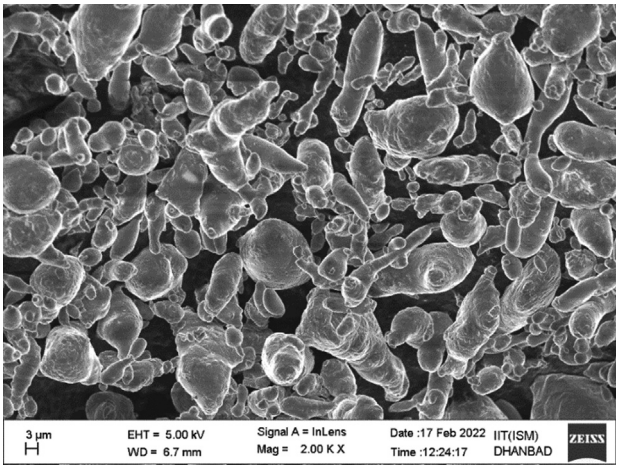

Fig. 1. FESEM image of the as-received aluminum powder.

of the peaks with the increase in milling time is seen in X-ray diffraction (XRD) patterns of ball-milled powders (Fig. 2a). In the ball milling process, the grinding media had an intensive impact on the microcrystalline powder, which resulted in a reduction of its grain size. The grinding balls created intense impacts, causing grains to rotate and subgrain boundaries to slide, resulting in an average grain size of 51.41 nm. In addition to the accumulation of dislocations, more new grains formed during milling, resulting in a decrease in average grain size from 133.32 to 51.41 nm (from 3 h to 65 h). A total broadening of the peaks was used to calculate crystallite sizes using the Williamson-Hall method (Eq. (1)). Fig. 2b illustrates the effect of milling time on crystallite size.

Fig. 3 displays TEM observations of the milled powder's microstructure after 65 h. The average grain size measure from TEM was 48.23 nm for aluminum powder milled for 65 h. The average crystallite size obtained from the XRD patterns (51.1 nm) is therefore compatible with the TEM-measured grain size and serves as a verification of the XRD grains' size. With the bright-field TEM images, the nanostructure of milled powders and polycrystallinity were also determined. The SAD pattern of Fig. 3c (corresponding to the area in Fig. 3a) reveals concentric ring patterns and sharp spots, concluding that the material is polycrystalline. Engineering stress–strain curves of nc-Al at the different strain rates are shown in Fig. 4. The figure also includes a engineering stress–strain curve of CG-Al at the strain rate of 0.01 s^{-1}. From Fig. 4, it can be seen that there exists a significant increase in the ultimate strength of nc-Al in comparison to the coarse-grained counterpart. This can be explained by the classical Hall–Petch relationship. Hall-Petch's relationship suggests that refinement of grains occurs when dislocation movement becomes constrained and also due to the stress concentration resulting from the accumulation of dislocation pile-ups. This explains the exceptional properties of nc-Al compared to CG-Al. The ultimate tensile strength of nc-Al reached a value of 371 MPa, which is 163% higher than that of CG-Al. Fig. 4a shows that the curve with a rate of 0.0001 s^{-1} exhibits a greater elongation, but lower strength. This decrease in strength can be due to the coarsening of the grains as a result of the long milling time. It is notable in Fig. 4a that higher strain rates result in increased strength. The strain at failure, however, decreases with the increasing strain rates. To examined the rate dependence of nc-Al, strain-rate sensitivity parameter (m) was determined. Several specimens were tested at strain rates of 0.01 s^{-1}, 0.001 s^{-1}, 0.0001 s^{-1} and m were determined according to:

$$m = \frac{\partial \ln(\sigma)}{\partial \ln(\dot{\epsilon})}$$

where $\dot{\epsilon}$ and σ are the strain rate and corresponding tensile strength, respectively. The strain rate sensitivity parameter was estimated as 0.035, which represents an eight-fold increase compared to coarse-grain Al (0.004).

3.2. Constitutive modeling

3.2.1. Summary of the constitutive theory

This section elaborates on a continuum-based constitutive theory which was recently developed by Wei and Anand [13]. The constitutive model is formulated in a hyperelastic-based finite deformation setting wherein shear, and cavitation-induced deformation micromechanisms are accounted for by proposing a plastically dilatant and non-normal flow rule. The plastic dilatancy features of nc-Al are reminiscent of the cohesive granular material that provide the primary physical motivation for the current development.

- *Stress–strain relation:* The stress can be determined using the free energy density per unit volume of intermediate space ψ as follows:

$$\mathbf{T}^e = \frac{\partial \psi(\mathbf{E}^e)}{\partial \mathbf{E}^e} = 2G(\mathrm{dev}\mathbf{E}^e) + K(\mathrm{tr}\mathbf{E}^e)\mathbf{I} \tag{1}$$

where

$$\psi(\mathbf{E}^e) = G|\mathrm{dev}\mathbf{E}^e|^2 + K\left(\mathrm{tr}\mathbf{E}^e\right)^2 \tag{2}$$

here K and G denote the bulk and elastic shear moduli.

- *Dilation based non-normal flow rule:* The expression for the evolution of the plastic deformation gradient is given by

$$\dot{\mathbf{F}}^p = \mathbf{D}^p\mathbf{F}^p \quad \text{such that} \quad \mathbf{F}^p(\mathbf{X}, 0) = \mathbf{I} \tag{3}$$

Let the plastic stretch rate be defined as

$$\mathbf{D}^p = (\mathbf{D}^p)_s + (\mathbf{D}^p)_c \tag{4}$$

with $(\mathbf{D}^p)_s$ being the shear-induced and $(\mathbf{D}^p)_c$ being the cavitation-induced deformation. The shear-dominated contribution can be represented as:

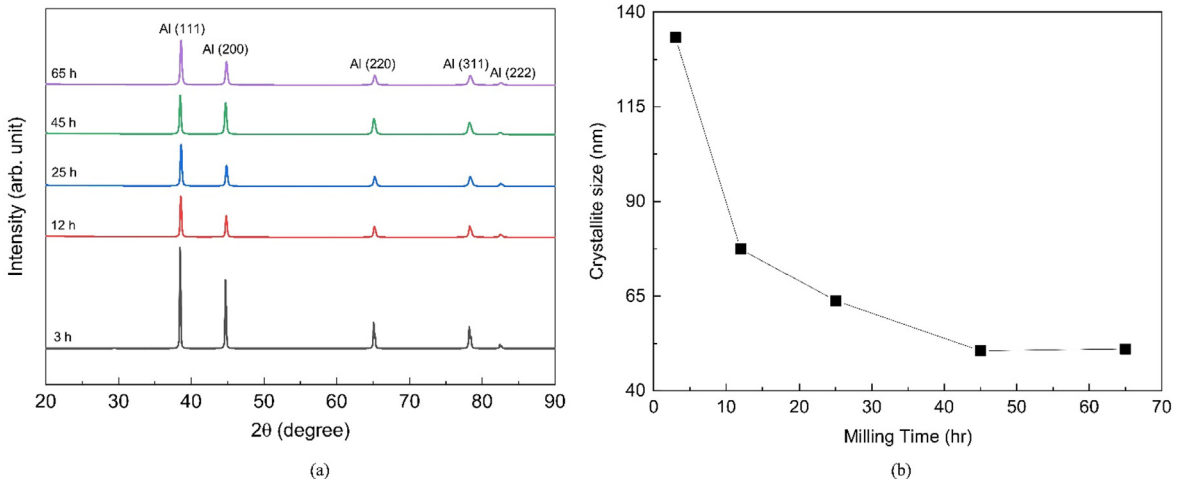

Fig. 2. (a) XRD patterns of ball milled Al powder with milling time; (b) Crystallite size variation with milling time.

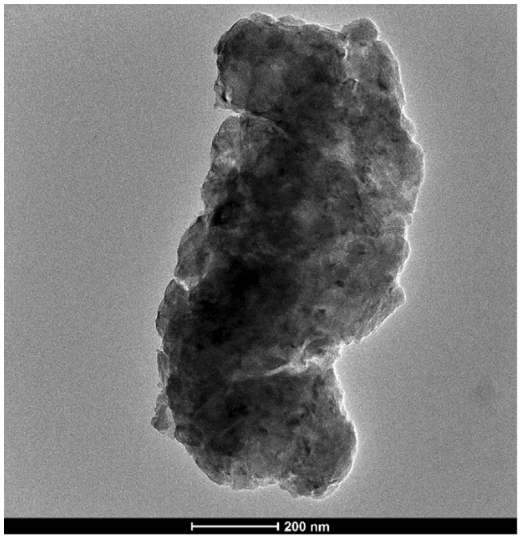

(a)

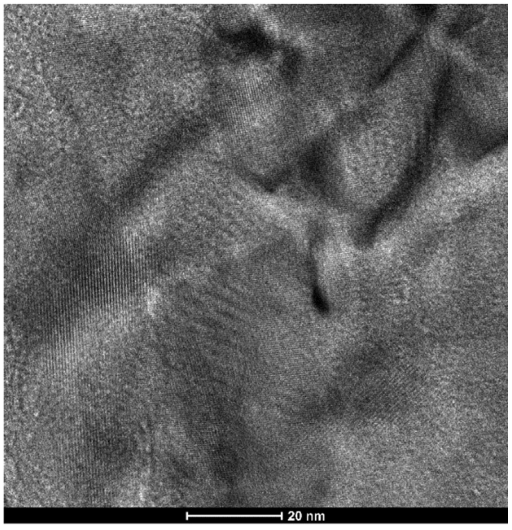

(b)

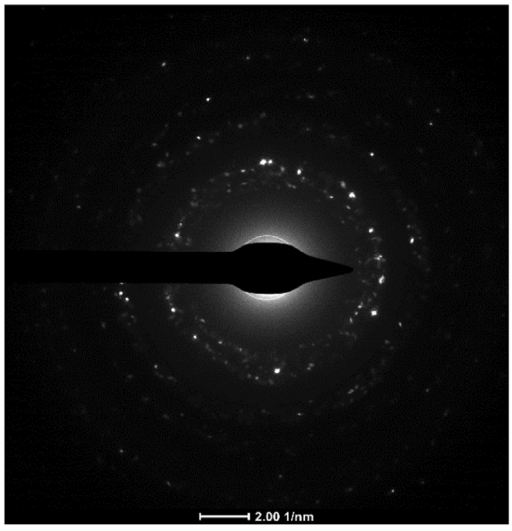

(c)

Fig. 3. TEM images of the (a), b) microstructure of milled Al powder for 65 h, and it's (c) associated SADP pattern.

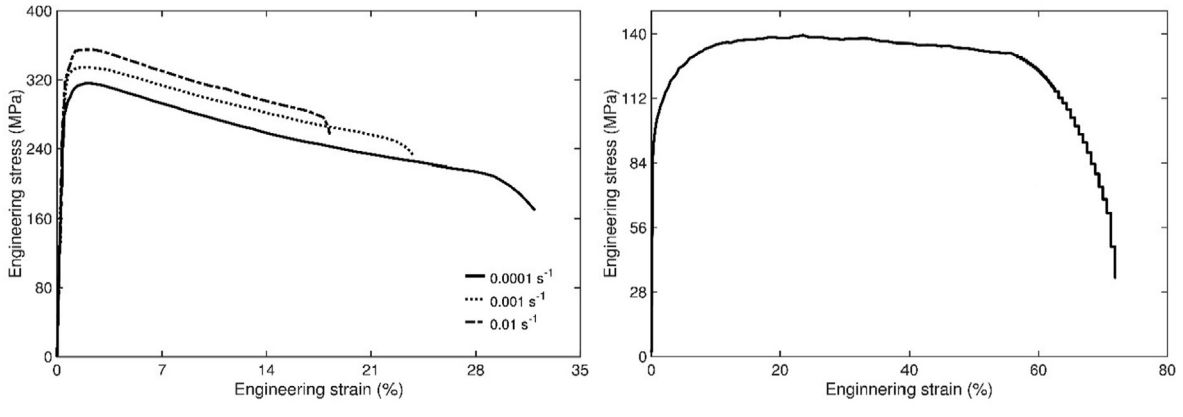

(a) (b)

Fig. 4. (a) Engineering stress–strain curves in tension for nc-Al at different strain rates, (b) Engineering stress–strain curves of CG-Al at the strain-rate of 0.01 s^{-1}.

$$(\mathbf{D}^p)_s = \mathrm{dev}(\mathbf{D}^p)_s + \frac{1}{3}\mathrm{tr}(\mathbf{D}^p)_s\mathbf{I} \tag{5}$$

with

$$\mathrm{dev}(\mathbf{D}^p)_s = d^p\mathbf{N}^p \mathrm{and} \mathrm{tr}(\mathbf{D}^p)_s = \beta d^p. \tag{6}$$

Here the variables $d^p = \sqrt{2}|\mathrm{dev}\mathbf{D}^p|$ and $\mathbf{N}^p = \mathrm{dev}\mathbf{T}^e/2\,\bar{\tau}$ represent the equivalent shear plastic strain rate, and the direction of deviatoric plastic flow, respectively. The equivalent plastic shear strain rate is determined by the respective relations

$$d^p = d_0\left[\frac{\bar{\tau}}{c + \mu\,\bar{p}}\right]^{1/m} \tag{7}$$

with $\bar{\tau} = |\mathrm{dev}\mathbf{T}^e|/\sqrt{2}$ and $\bar{p} = -\frac{1}{3}\mathrm{tr}\mathbf{T}^e$ denote the equivalent shear stress and the mean-normal pressure, respectively. The quantities $c > 0$ and $\mu \geq 0$ being cohesion internal variable and friction internal variable, respectively. Moreover, $d_0 > 0$ and $m > 0$ stand for the reference plastic shear strain rate and the strain-rate sensitivity parameter, respectively.

The quantity β is proposed in the form of:

$$\beta = g_0\left[1 - \frac{\eta}{\eta^*}\right] \tag{8}$$

where $g_0 > 0$ and $\eta^* > 0$ are the material constitutive parameters that can be experimentally determined. The cavitation-induced deformation is now introduced:

$$(\mathbf{D}^p)_c = \sum_{i=1}^{3} d_c^{(i)}(\hat{\mathbf{e}}_1 \otimes \hat{\mathbf{e}}_1) \tag{9}$$

such that

$$d_c^{(i)} = d_0\left[\frac{< \sigma_i - \sigma_{th} >}{\sigma_{cr}}\right]^{1/m} \tag{10}$$

here the quantities σ_i denotes the eigenvalues of the stress tensor. The expression $< A >$ denotes the Macaulay bracket notation such that $< A >= (1/2)(|A| + A)$.

- *Kinetic rate-formed equations of internal variables:* The internal friction is assumed to be constant i.e., $\dot{\mu} = 0$. Substituting (9) and (5) into (4) yields

$$\dot{\eta} = \mathrm{tr}\mathbf{D}^p = g_0\left[1 - \frac{\eta}{\eta^*}\right]d^p + \sum_{i=1}^{3} d_c^{(i)} \;\text{ with }\; \eta(0) = 0 \tag{11}$$

The expression for the evolution equation for the cohesion parameter is given by

$$\dot{c} = \left[h_0|1 - \frac{c}{c^*}|^a \,\mathrm{sign}\left(1 - \frac{c}{c^*}\right)\right]d^p - h_c\sum_{i=1}^{3} d_c^{(i)} \tag{12}$$

where

$$c^* = \bar{c}\left[\frac{d^p}{d_0}\right]^n + b(\eta^* - \eta) \quad \text{and} \quad c(0) = c_0. \tag{12}$$

In summary, the material parameters which are needed to be determined from experiments are

$$\left\{G, K, d_0, h_0, n, c_1, \sigma_{th}, m, a, b, c_2, h_c, \mu, c_0, \eta^*, \bar{c}, g_0\right\}$$

The constitutive theory is implemented into the Abaqus/Explicit finite element solver using a vectorized user-material subroutine interface. This is done using an explicit-based numerical time integration scheme. To avoid inaccuracies caused by solution instability, careful consideration is given to the size of time steps used in finite element simulations. The explicit setting of integration schemes does not require the Newton-Raphson iterations, which makes the solution method for the constitutive equations fast and agile.

3.2.2. Material parameters identification procedure

A procedure for determining material constants $\left\{G, K, d_0, h_0, n, c_1, \sigma_{th}, m, a, b, c_2, h_c, \mu, c_0, \eta^*, \bar{c}, g_0\right\}$ in constitutive theory, from physical experiments, are outlined in this section. The parameters $\{G, K\}$ can be estimated fairly well from the bulk coarse-grained Al data. The elastic shear modulus, G = 26 GPa, and the elastic bulk modulus, K = 76 GPa, were obtained from Ledbetter [15] at room temperature. The referential strain rate, d_0, is set to the lowest strain rate in the conducted simple tensile experiment. The parameters c_0 and η controlling the initial strength and the stabilized flow stress under shearing can be identified by fitting the model to the simple stress–strain curve obtained from a simple tensile experiment. The value of c_0 was obtained as140 MPa. The parameters $\{b, g_0, \eta^*\}$ can be calibrated by fitting the model to the strain-softening portion of the curve caused by shear-induced dilatancy. The obtained values of b, g_0, η^* were 19 GPa, 0.006 GPa, and 0.002 GPa, respectively. The friction coefficient can be approximated by comparing the flow strength between tension and compression experiment test data and the referential strain rate and found out as 0.03. Stress–strain curves at various strain rates can be used to determine the values of the parameters m and n governing the rate-sensitivity features of the model. The values of m and n were 0.043 and 0.04, respectively. For the purpose of simplicity, the parameters σ_{th} and h_c are set to zero because there aren't any experimental reports available for the estimation of these parameters. Additionally, fitting the model to experimental settings like the notched bar tension test, where cavitation effects are prominent, is the best way to identify the cavitation-related parameters $\{c_1, c_2\}$ However, we estimate the parameters using the values given for a Mg-based nanocrystalline [13] as a first-cut assumption. The values of c_1, c_2 were taken as 2.5 GPa and 11, respectively. All the material parameters were obtained from the true stress–strain curves of nc-Al at different strain rates. The true stress–strain curves of nc-Al along with evaluation of the material parameters has been addressed in-depth elsewhere.

3.2.3. Tension test simulations

In this part, the uniaxial stress–strain response derived from a simple uniaxial tension test is predicted using the constitutive theory appropriately calibrated for nc-Al. Reiterating that the experiment was carried out on a sample with a dog-bone shape having a gauge diameter and gauge length of 4 mm and 20 mm, respectively, prepared in accordance with ASTM E8/E8M-13a. The engineering stress–strain prediction from the finite element simulation is compared to the experimental stress–strain data from the tension test, which was performed at different strain rates of 0.01 s^{-1}, 0.001 s^{-1} and 0.0001 s^{-1}. The constitutive theory and its finite element implementation can represent the rate-sensitive features of the nc-Al so that the flow stress increases with the increase in strain rate, as is shown in Fig. 5. Additionally, the test data acquired from the simple uniaxial tension tests are in good accord with the results acquired from the finite element simulation. It is important to note that the Abaqus reduced-integration continuum three-dimensional brick (C3D8R) element was used to generate the finite element simulation results seen in Fig. 5.

4. Conclusion

In the present study, nc Al was synthesized using in-situ hot extrusion and high-energy ball milling of microcrystalline Al powder. The tensile characteristics of nc-Al was investigated and cor-

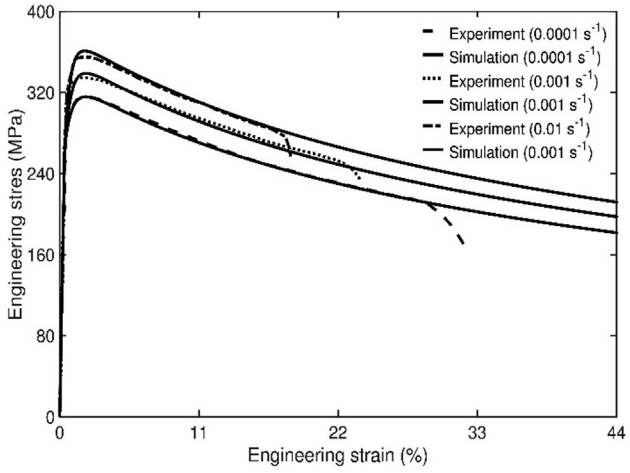

Fig. 5. Comparison of experimental and numerical results for nc-Al in tension at different strain rates.

roborated with its nanostructure. nc-Al showed a significant improvement in its ultimate tensile strengths and ductility. nc-Al showed a maximum ultimate strength of 371 MPa, which is 163% percent higher than that of coarse-grained Al. Moreover, nc-Al exhibited a strain rate sensitivity of 0.035, which is eight times more than coarse-grained Al (0.004). Further, an isotropic rate-dependent plasticity approach based on continuum-level modeling has been proposed. A vectorized user material code has been implemented into the Abaqus/Explicit for the modeling of nc-Al. After suitable calibration of the material parameters, it was found that the constitutive model developed can successfully model the mechanical response of nc-Al.

CRediT authorship contribution statement

Surja Deka: Methodology, Formal analysis, Visualization, Investigation, Validation, Writing – original draft. **Farzin Mozafari:** Methodology, Formal analysis, Investigation, Software, Writing – review & editing. **Ashis Mallick:** Conceptualization, Resources, Supervision.

Data availability

Data will be made available on request.

Declaration of Competing Interest

The authors declare the following financial interests/personal relationships which may be considered as potential competing interests: [Ashis Mallick reports financial support was provided by DST India.]

Acknowledgements

S.D., and A.M. sincerely acknowledge the financial support from ASEAN-Indian science and technology development fund, DST, Govt. of India, vide grant no. IMRC/AISTDF/RND/P14/2018

References

[1] K.M. Youssef, M.A. Abaza, R.O. Scattergood, C.C. Koch, High strength, ductility, and electrical conductivity of in-situ consolidated nanocrystalline Cu-1% Nb, Mater. Sci. Eng. A 711 (2018) 350–355.
[2] I. Sabirov, M.Y. Murashkin, R.Z. Valiev, Nanostructured aluminium alloys produced by severe plastic deformation: New horizons in development, Mater. Sci. Eng. A 560 (2013) 1–24.
[3] A. Mohammadi, N.A. Enikeev, M.Y. Murashkin, M. Arita, K. Edalati, Examination of inverse Hall-Petch relation in nanostructured aluminum alloys by ultra-severe plastic deformation, J. Mater. Sci. Technol. 91 (2021) 78–89.
[4] R.Z. Valiev, T.G. Langdon, Principles of equal-channel angular pressing as a processing tool for grain refinement, Prog. Mater Sci. 51 (7) (2006) 881–981.
[5] A.P. Zhilyaev, T.G. Langdon, Using high-pressure torsion for metal processing: Fundamentals and applications, Prog. Mater Sci. 53 (6) (2008) 893–979.
[6] J.K. Rana, D. Sivaprahasam, K.S. Raju, V.S. Sarma, Microstructure and mechanical properties of nanocrystalline high strength Al–Mg–Si (AA6061) alloy by high energy ball milling and spark plasma sintering, Mater. Sci. Eng. A 527 (1–2) (2009) 292–296.
[7] J. Christudasjustus, C.S. Witharamage, G. Walunj, T. Borkar, R.K. Gupta, The influence of spark plasma sintering temperatures on the microstructure, hardness, and elastic modulus of the nanocrystalline Al-xV alloys produced by high-energy ball milling, J. Mater. Sci. Technol. 122 (2022) 68–76.
[8] D. Guan, J. Gao, W.M. Rainforth, Effect of cryomilling time on microstructure evolution and hardness of cryomilled AZ31 powders, Mater Charact 178 (2021).
[9] A.S. Khan, Y.S. Suh, X. Chen, L. Takacs, H. Zhang, Nanocrystalline aluminum and iron: Mechanical behavior at quasi-static and high strain rates, and constitutive modeling, Int. J. Plast 22 (2) (2006) 195–209.
[10] A.S. Khan, B. Farrokh, L. Takacs, Effect of grain refinement on mechanical properties of ball-milled bulk aluminum, Mater. Sci. Eng. A 489 (1–2) (2008) 77–84.
[11] S. Whalen, M. Olszta, C. Roach, J. Darsell, D. Graff, M. Reza-E-Rabby, T. Roosendaal, W. Daye, T. Pelletiers, S. Mathaudhu, N. Overman, High ductility aluminum alloy made from powder by friction extrusion, Materialia. 6 (2019).
[12] R. Dobosz, M. Lewandowska, K.J. Kurzydlowski, The effect of grain size diversity on the flow stress of nanocrystalline metals by finite-element modelling, Scr. Mater. 67 (4) (2012) 408–411.
[13] Y. Wei, L. Anand, A constitutive model for powder-processed nanocrystalline metals, Acta Mater. 55 (3) (2007) 921–931.
[14] T. Shimokawa, A. Nakatani, H. Kitagawa, Grain-size dependence of the relationship between intergranular and intragranular deformation of nanocrystalline Al by molecular dynamics simulations, Phys. Rev. B 71 (22) (2005).
[15] H.M. Ledbetter, R.P. Reed, Elastic properties of metals and alloys, I. Iron, nickel, and iron-nickel alloys, J. Phys. Chem. Ref. Data 2 (3) (1973) 531–618.